Heliyon 9 (2023) e12601

Contents lists available at ScienceDirect

Heliyon

journal homepage: www.cell.com/heliyon

Research article

Bioenergetics of the polyphosphates accumulation in *Pseudomonas aeruginosa* via polyphosphate kinase activation by choline in a lung colonization model

Alejandro Rossi [a,b], Sandra Grumelli [a,c,*]

[a] *Department of Molecular Biology, Universidad Nacional de Rio Cuarto, Córdoba, Argentina*
[b] *Rizobacter Argentina, Buenos Aires, Argentina* [1]
[c] *Center of Investigation in Medicine of Respiration, (CIMeR), Córdoba, Argentina* [1]

ARTICLE INFO

Keywords:
Pseudomonas aeruginosa
Rhizosphere
Lung
Cystic fibrosis
Choline
Succinate
Inorganic polyphosphates
Phosphatase
Kinase
ATP
Energy flow
Kinetic of enzymes

ABSTRACT

Pseudomonas aeruginosa is an ubiquitous and opportunistic bacteria found in water, soil, plants, and immunocompromised humans. Cystic fibrosis (CF) patients are the most vulnerable population to lung colonization by these bacteria. Upon infection, choline and succinate are released from the CF lungs and are catabolized by *P. aeruginosa*. The bacteria accumulate inorganic polyphosphates, rather than succinate, when choline is catabolized, producing physiological and morphological changes leading to ineradicable infection. Thus, we sought to quantify the enzymes responsible for polyphosphate accumulation and to determine how choline catabolism affects energy flow and storage. Subcellular fractions showed that exo-polyphosphate phosphatase (PPX) activity resides mainly in the periplasm, and three isoenzymes of 24, 70, and 200 KD were found. The PPX activity in the periplasm of bacteria grown with choline was inhibited in an anti-competitive manner from Km 0.5 to 1 μM, and their Vmax increased from 50 to 100 nmol $PO_4^{\equiv}$/min/g of protein in succinate medium. Since PPX inhibition by choline did not explain the 3.8-fold increase in polyphosphates, we quantified the polyphosphate kinase activity, and its significant 2.4-fold increase was consistent with the accumulation. Furthermore, intracellular ATP concentration directly correlated with the energetic yield of the carbon source and was significantly higher for succinate, suggesting that the restriction of energy caused by choline catabolism may induce morphological and physiological changes to the swarm form thus facilitating their migration and tissue colonization

1. Introduction

Pseudomonas aeruginosa is an ubiquitous bacteria found in water, soil, plants´ rhizospheres, and humans. In plants, *P. aeruginosa* occurs at a ratio of 1:4 with the *Rhizobium* [1] and promotes growth-producing siderophores, such as pyocyanin, indole-3-acetic acid, and phosphate solubilization which, enhances seed germination and seedling vigor *in vitro* [1].

As a respiratory pathogen, *P. aeruginosa* encounters choline and succinate and can utilize these as a carbon source [2]. It was previously demonstrated that mice modeled with *P. aeruginosa* infections after intranasal lipopolysaccharide (LPS) treatment, to mice

* Corresponding author.
E-mail address: sgrumelli@yahoo.com (S. Grumelli).
[1] Current address.

https://doi.org/10.1016/j.heliyon.2022.e12601
Received 3 March 2022; Received in revised form 6 October 2022; Accepted 15 December 2022

Available online 30 December 2022

with cigarette-induced emphysema [3]. Choline challenges to the lung of these mice reproduced the physiological conditions of acidosis, hypercapnia, and hypoxia of human exacerbations suggesting this is a good model of acute lung exacerbations [3]. *In-vitro* studies showed that choline versus succinate catabolism by *P. aeruginosa* is associated with polyphosphate ($(PO_4^-)_n^=$) accumulation and replicates the bacteria recovered from the lungs of patients with cystic fibrosis (CF) [3,4]. $(PO_4^-)_n^=$ may contribute to *P. aeruginosa* pathogenesis by disrupting the vascular barrier, cleaving the endothelium and promoting invasion [5–8], inhibiting C1, C5, and factor XII from the complement cascade, and suppressing innate immunity [9,10].

Bacterial $(PO_4^-)_n^=$ are polymers of phosphate ($PO_4^{\equiv}$) from 5 to 1000 s units that form intracellular magnet-sensitive inclusions that contain magnesium, calcium, cobalt, chromium, or iron (Mg^{+2}, Ca^{+2}, Co^{+2}, Cr^{+2}, or Fe^{+2}) [11–13] and play key roles in stress response, swimming, and swarming, which are essential activities for bacterial infection and colonization [14]. $(PO_4^-)_n^=$ accumulation occurs as a result of choline catabolism [3] that may occur through inhibition of the degradation of $(PO_4^-)_n^=$ to $PO_4^{\equiv}$ by exo-polyphosphate phosphatase (PPX) or synthesis via ATP addition to $(PO_4^-)_n^=$ by activation of polyphosphate kinase (PPK). Since $(PO_4^-)_n^=$ is essential for swarming and antibiotic resistance, [15,16] we sought to determine which enzyme is responsible for this accumulation because this process enhances bacterial virulence and cleaves the endothelial barrier thus facilitating bacterial access to the tissue and eliciting inflammation [17–19]. Thus, controlling $(PO_4^-)_n^=$ accumulation may reduce the bacterial capability to colonize the CF lung. In this study, we show that PPX activity occurs in the cytoplasm, membrane, and periplasm, in which it was found to be significantly higher. Periplasmic PPX has acid (pH 5.8) and alkaline phosphatase activity (pH 9.2) with a higher affinity for polyphosphates with longer chains. The kinetic data indicate that more than one PPX enzyme was active which is consistent with the purification of 3 isoenzymes with PPX activity. PPX activity was found to be higher in the periplasm from the choline medium, and the PPK membrane activity was significantly higher relative to succinate, indicating PPK activation is mainly responsible for $(PO_4^-)_n^=$ accumulation. Overall, polyphosphate accumulation represented 1.3% of the total phosphate and 2.9% of the total ATP [3]. Thus, the energy accumulated as polyphosphate is negligible compared to that stored as phospholipids and other macromolecules. We also found that choline produces a significant energetic restriction that may lead to the swarm form.

2. Materials and methods

2.1. Bacterial growth

P. aeruginosa Fildes III strains were grown at 37 °C in Luria Bertani (LB) Broth (10 g of tryptone, 5 g of yeast extract, and 5 g of NaCl per liter of H_2O). For experiments, high phosphate liquid saline culture containing 22 mM KH_2PO_4, 17 mM Na_2HPO_4, 8.5 mM NaCl, and 0.8 mM $MgSO_4$ with either 20 mM of choline, betaine, dimethylglycine, or succinate as the carbon source plus 18.7 mM ammonium chloride (NH_4Cl) [3] were inoculated with 1% (v/v) with *P. aeruginosa* and grown overnight in LB. These cultures were grown in parallel in Erlenmeyer flasks with medium composing 1/10 of the flask volume and grown at 37 °C with agitation at 100 rpm. *P. aeruginosa* were harvested during late exponential growth and had an optical density (OD) at 660 nm of 0.8 to 1.0. We used absorbance at 660 versus 595 nm to avoid pyocyanin absorption [23]. The total protein was quantified in 60 μl of bacterial culture mixed with 240 μl of 1 M NaOH and warmed to 90 °C for 20 min. Subsequently, the protein concentration was quantified in 100 μl of this mixture, using the method of Bradford [20]. The remaining *P. aeruginosa* culture was centrifuged at 10,000 g for 10 min, the pellet was washed twice with saline solution, and weighed.

2.2. Sub-cellular extracts

The sub-cellular fractions were extracted as described by Ames et al. [21]. Briefly, bacterial pellets were collected, treated with 10 μl chloroform per 1 ml of culture medium, shaken for 15 min, and then resuspended in 10 ml of 10 mM Tris-HCl buffer, pH 8. The suspension was centrifuged at 10,000 g for 10 min, and the supernatant containing the periplasmic fraction was removed and saved. The pellet was resuspended in distilled water, shaken, and centrifuged for 20 min at 15,000 g, the supernatant contained the cytoplasmic fraction, and the pellet consisting of the membrane enzymes were separately resuspended in 0.9% NaCl in trice-distilled H_2O. The total protein in each extract was quantified by Bradford assay [20].

2.3. Quantification of the enzymatic activities

The exo-polyphosphate phosphatase activity (PPX) in the periplasm, membrane, and cytoplasm was measured according to a specific protocol. The reaction solution contained 100 mM acetate buffer pH 5.0, 2 mM $MgCl_2$, 10 mM KCl, and 5 μM of polyphosphate n = 79 units ($(PO^-_4)_{79}^=$), as substrate, unless otherwise specified. We added 470 μl of this mix to 30 μl of periplasmic extract, controlled for protein concentration, and incubated at 37 °C for 40 min. The reaction was terminated with 250 μl of 30% TCA acid, and the $PO_4^{\equiv}$ released was quantified using the method of Fiske [22] and detected at 660 nm.

The reaction buffers used to determine the pH optima for PPX activity were 100 mM of sodium acetate/acetic acid (pH 3.5–5.5), HEPES (pH 6.5–7.4), boric acid/borax (pH 7.5–8.9), or borax/sodium hydroxide (pH 9.2–10). The effect of each cation on PPX activity was measured using a solution of 1.5 mM final concentration.

The activity of the periplasmic marker, acid phosphatase (AcPase) [23], was quantified in 500 μl of a reaction mix containing 100 mM acetate buffer at pH 5.0, 2 mM $MgCl_2$, and 10 mM para-nitro phenyl phosphate substrate. Ten microliters of the periplasmic extract were added to the reaction mix and incubated for 15 min at 37 °C. The reaction was terminated with 500 μl of 2 M NaOH, and the product detected at 410 nm [23].

PPK activity was measured from membrane extracts [24] as described by Robinson and Wood [25]. The activity was measured using a coupled reaction in which ATP was regenerated by pyruvate kinase and nicotinamide adenine dinucleotide (NADH) consumption. The reaction solution contained 40 mM HEPES pH 8.0, 6 mM $MgCl_2$, 2 mM phosphoenolpyruvic acid (PEP), 0.5 mM NADH, 2.4 mM ATP-Mg^{+2}, 10 U pyruvate kinase, 10 U lactate dehydrogenase and 0.5 mg/ml polyphosphate of n = 45 units ($(PO^{-}{}_4)_{45}{}^{=}$) as substrate added to the membrane extracts to a final volume of 0.9 ml at 37 °C [21]. The reaction was followed at 340 nm in a Beckman DU 640 spectrophotometer. One unit of PPK was considered the amount of enzyme that catalyzes the release of 1 μmol of ADP/min/ml.

2.4. Enzyme kinetics

To understand the mechanism of polyphosphate degradation by PPX we considered that the enzyme binds the substrate, and its concentration is negligible compared to the substrate. Assuming a pseudo-first-order reaction, we can consider the complex enzyme–substrate to be in a steady-state. We utilized the Michaelis–Menten equation to write the global velocity equation for $(PO_4{}^{-})_n{}^{=}$ degradation. The Michaelis–Menten constant (Km) was then quantified using Lineweaver–Burk analysis.

The deviation of the modeled velocity values from the measured ones, for each n, was determined as in Eq. (1).

$$|\varepsilon|\% = \sqrt{\left((\mathrm{Vtheorical}\, n - \mathrm{Vmax}n) * \frac{100}{\mathrm{Vmax}n}\right)^2} \tag{1}$$

2.5. Purification of polyphosphate phosphatase

The periplasmic extract was used for PPX purification as the activity is significantly higher in this compartment. Briefly, bacteria grown to the early stationary phase were centrifuged at 8000 g for 10 min, and the pellet was washed with 155 mM NaCl. The periplasmic extracts were obtained by adding 10 μl of chloroform per ml of culture, and vortexed for 15 min after which 10 volumes of 10 mM Tris-HCl pH 8.0 were added. The samples were centrifuged at 10,000 g for 10 min, and the supernatant, containing the periplasmic enzymes, was used for protein purification.

The purification procedure comprised three steps [26]: (1) differential precipitation with ammonium sulfate, (2) separation by molecular weight filtration column in an FPLC, and (3) separation with a hydroxyapatite column.

2.5.1. Step 1. Precipitation with ammonium sulfate

The enzymatic activity present in the periplasmic fraction was separated by fractional precipitation with solid ammonium sulfate, as previously described [26]. The enzymatic extract was kept on ice throughout the whole procedure and maintained at pH 7.4 by 1M NH_4OH addition. Solid $(NH_4)_2SO_4$ was added in 10% increments to obtain subsequent precipitations at 20% to 100% saturation. After 15 min of stirring, the suspension was centrifuged at 25,000 g for 20 min at 4 °C. The pellet was dissolved in 10 mM Tris-HCl, pH 8.0, and $(NH_4)_2SO_4$ was added to the supernatant to obtain the next fraction. The major PPX activity occurred in 30%, 70%, and 90% saturation fractions.

2.5.2. Step 2. Separation by molecular weight

The fractions from step 1, which had more enzymatic activity, were resuspended in 10 mM Tris-HCl pH 8.0, centrifuged, and filtered with millipore 0.5 μm filters after which 0.3 ml was added to an FPLC fitted BioSep-Sec-S 300 (4 mm × 300 cm) column, pre-equilibrated with 10 mM Tris-HCl pH 8.0 and eluted with 10 mM Tris-HCl, pH 8.0 at a constant flow of 0.5 ml/min. The proteins were detected by a detector Uv-Vis at 280 nm. Samples of 1 ml were collected, and 250 μl were assayed for PPX activity after addition of 250 μl acetate buffer pH 5.0 with 2 mM $MgCl_2$, incubated at 37 °C, and quantified by the method of Fiske–Subarrow [22]. A molecular weight curve was generated with the molecular filtration column described and molecular weight markers from Bio-rad (Blue Dextran 2 000, β-amylase 200, alcohol dehydrogenase 150, albumin 66, carbonic anhydrase 29, and cytochrome C 12,4 Kilo Daltons [KD]).

2.5.3. Step 3. Purification by hydroxyapatite

PPX activity occurred in fractions with molecular weights of approximately 200, 70, and 24 KD. These were further separated by a hydroxyapatite (HTP) (Bio-Rad, Bio-Gel HTP Gel) column of a 10 mm by 10 mm diameter, that was equilibrated with 10 mM Tris-HCl at pH 8.0. One hundred microliters of sample were loaded and eluted with two volumes of the column of the following solutions in the given order: (1) 5 mM $MgCl_2$, (2) 150 mM NaCl, and (3) 500 mM NaH_2PO_4.

2.6. Quantification of the intracellular ATP

The intracellular concentration of ATP was determined using a luciferin–luciferase kit from Molecular Probes (A-6608). Briefly, 600 μl of a solution containing 25 mM tricine pH 7.8, 5 mM $MgSO_4$, 0.1 mM EDTA, 0.1 mM sodium azide, 1 mM dithiothreitol, 0.5 mM luciferin and 2.5 μl of 5 mg/ml luciferase, was added to 100 μl of sample. Light emission was quantified in a Spex Fluoromax spectrofluorometer at $\lambda = 560$ nm without previous excitation, and the emission was recorded for 300 s. The increment of emission from the background was plotted versus ATP concentration to obtain the calibration curve for 0.1, 1, 50, and 100 μM of ATP. One hundred microliters of intracellular extracts from bacteria grown with choline, succinate, acetate, or proline were used for ATP

quantification. The intracellular metabolites were obtained as previously described [27] by extraction of 10 ml of bacterial culture grown to OD 0.6–0.8 and centrifuged at 10,000 g for 5 min. The supernatant extract contained the intracellular metabolites. One hundred microliters of this extract were added to the tube and mixed, and the light emission was recorded for 300 s with slit 7. The average emission was constructed after subtracting the background emission, and the ATP concentration was calculated from the calibration curve.

The free energy from choline, or succinate, catabolism was calculated using the Hess law to obtain the combustion enthalpy, and the Gibbs law to calculate the free energy, for isothermic processes (37 °C), $\Delta G = \Delta Hc - T\Delta S$. The combustion heat ($\Delta H_c$) of the carbon source was determined using the semi-empirical program AMPAC 5.0. The calculated and measured values were compared to determine the standard error of the method, which was between 0.2% and 18% (Supplementary Table 1). The free energy obtained was $\Delta G°_{succinate} = -1556$ and $\Delta G°_{choline} = -871$ Kcal/mol, which yielded 213 and 119 mol of ATP, respectively.

3. Results

We demonstrated that choline causes changes in host and pathogen physiology, by producing exacerbation and increasing virulence, respectively [4]. *P. aeruginosa* significantly changed its macromolecular composition when choline is catabolized and led to an increase in inorganic polyphosphate. We were interested in the enzymes involved in its turnover and the energetic flow from the carbon source to the phosphate metabolism.

3.1. PPX characterization

To determine how choline affects $(PO^-_4)_n^=$ metabolism, we sought to quantify exo-polyphosphate phosphatase activity, which degrades $(PO^-_4)_n^=$ to $PO_4^{\equiv}$ [28], and the polyphosphate kinase (PPK) activity, which synthesizes $(PO^-_4)_n^=$ from adenosine-triphosphate (ATP) [29,24]. Choline induces periplasmic acid phosphatase (AcPase) in high phosphate medium when it is the only carbon source [23]. Thus, we used choline-induced AcPase as a marker of periplasm in high phosphate medium [30,31]. A significant increase in AcPase activity in the periplasmic fraction was found as expected compared to that in the cytoplasm or membrane (Fig. 1a top plot). PPX activity was also significantly higher in the periplasm than in cytoplasm and membrane fractions (Fig. 1a bottom plot). These results suggest that PPX activity is mainly periplasmic; thus, we characterized the pH optima for the PPX activity in the *P. aeruginosa* periplasmic fraction (Fig. 1b), which peaked at pH 5.8 and then again at pH 9.2. Since we wanted to assess the optimal conditions for PPX activity, periplasmic extracts at pH 5 were chosen because at pH 9.2 alkaline phosphatase activity, which is also a periplasmic enzyme, occurs [32].

To characterize the effects of cations on optimal PPX activity, we treated periplasmic fractions with several tri-, bi-, and monovalent metals (Fig. 1c). The stronger activators were Zn^{+2}, Mn^{+2}, and Mg^{+2}, indicating a radius versus charge ratio (r/q) of 0.27 as the binding site size in the enzyme. Conversely, Ce^{+3}, Fe^{+3}, Fe^{+2}, Co^{+2}, and Cu^{+2} cations with an r/q ratio between 0.16 and 0.27 were strong inhibitors of PPX because they may compete for the same binding site thus producing competitive inhibition. The monovalent cations, Li^+, Na^+, and NH_4^+, were also inhibitors but to a lesser degree than tri- or bi-valent cations probably because their $r/q \geq 0.27$; these cations are 2 to 6 times bigger than the binding site of Mg+2; thus, they may bind elsewhere, and their inhibition may be anti-competitive. The activators Mg^{+2}, Mn^{+2}, and Zn^{+2} have similar electronic configurations; all of them have lost two electrons in the S orbital. Seventy-two percent activation of PPX was produced by Mg^{+2}, which has a cubic crystal structure without electrons on the d-orbital of the external layer, while the hexagonal crystal structure of Mn^{+2} and Zn^{+2} with electrons in 3d and 4d orbitals produced 89% and 50% PPX activation, respectively, which was not significantly different ($p = 0.3$) than Mg^{+2} activation. This finding suggests that small cubic structures, such as Mg^{+2}, form a perfect match with the binding site in PPX. However, this cation binding site is also susceptible to inhibition by smaller metals of $r/q \leq 0.27$, such as Fe^{+3}, Fe^{+2}, Co^{+2}, and Cu^{+2}, which are small enough to compete for the binding site.

After determining the optimal Mg^{+2} concentration required for PPX activity, we measured the initial velocity for different volumes of extract (10, 20, and 40 μl) and times of 0, 20, 40, and 60 min at pH 5.0, 37 °C and protein concentration below 5 mg/ml of periplasmic extracts (data not shown).

3.2. PPX has a higher affinity for longer polyphosphates

We sought to establish the substrate with the highest affinity for PPX. Since $(PO_4^-)_n^=$ can have from 3 to more than 1000 units, we tested the PPX activity at varying concentrations of $(PO_4^-)_n^=$ of different lengths, $n = 3$, 5, 18, 27, 46, and 79 units in a range of 3 to 300 μM to assess their affinity constant for the enzyme (K_m) and their maximal velocity (V_{max}). Fig. 2a shows that $(PO_4^-)_n^=$ of $n = 5, 18, 27$, and 46 led to a significant increase in PPX activity at all tested concentrations, while $n = 79$ showed high affinity but was inhibitory at the highest concentration. Their K_m was then quantified using the Lineweaver–Burk plots (Fig. 2a below), and verified by Edie–Scatchard and Hanes–Wolf plots (data not shown); the representative plot for $(PO_4^-)_{79}^=$, shows two slopes, a high-affinity K_{m1} and a low-affinity K_{m2} for every length of $(PO_4^-)_n^=$ of $n > 3$ tested, suggesting more than one PPX enzyme was present. The downward concave in the double reciprocal plots are characteristic of enzymes with substrate activation, negative cooperation of polymeric enzyme, or multiple enzymes catalyzing the conversion of a common substrate [33]. We also determined V_{max}, and the slope (K_m/V_{max}) for every length of $(PO_4^-)_n^=$ and represented these parameters versus the length (n) as shown in Fig. 2b, The K_m decreased with the square root of n (Fig. 2b, left top) for both high or low K_m series, which suggested that their affinity for PPX increased with the $(PO_4^-)_n^=$ length. The regressions that fit both K_m series were quadratic equations, and parallels separated by 46

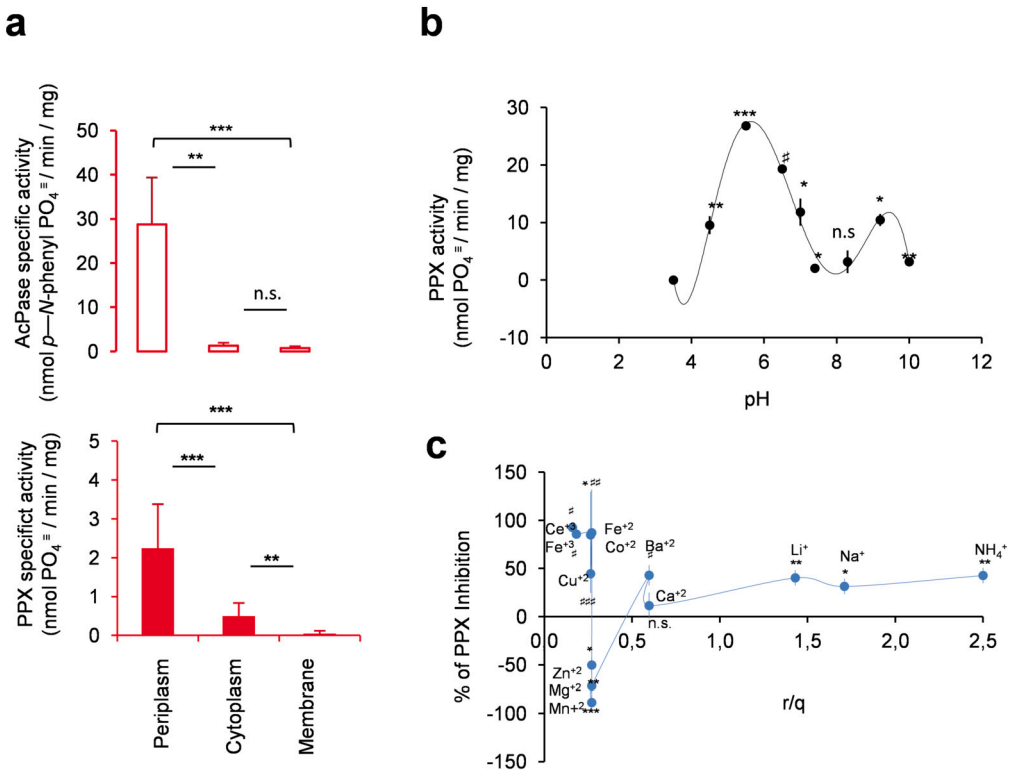

Fig. 1. Characterization of Exo-Polyphosphate Phosphatase (PPX) activity. **(a)** Intracellular localization of PPX activity using Acid Phosphatase (AcPase) as a periplasmic marker (n = 6 independent experiments). **(b)** Changes of PPX activity with pH quantified in periplasm extracted from *Pseudomonas aeruginosa* grown with choline. The buffer solution used was 100 mM, and to vary the pH we used sodium acetate /acetic acetate (pH 3.5–5.5), HEPES (pH 6.5–7.4), boric acid/borax (pH 7.5–8.9) and borax/sodium hydroxide (pH 9.2–10), (n = 3 independent experiments). **(c)** Effect of metal, radius to charge ratio (r/q), on PPX activity. Representative plot of the PPX activity, from the periplasm of *P. aeruginosa*, quantified at pH 5 for 40 minutes at 37 °C versus the activity relative to 2 mM $MgCl_2$ plus 1.5 mM ions. The phosphate released by the PPX from 5 μM $(PO_4^-)_{45}^=$ was quantified using the method of Fiske [22]. Throughout, the data are expressed as mean ± standard error of the mean (s.e.m). Student's T-test values for one tail, unequal variances, relative to the previous data point, were: n.s, $p \geq 0{,}05$; $^{*}p \leq 0{,}05$; $^{**}p \leq 0{,}01$; $^{***}p \leq 0{,}005$; $^{\#}p \leq 0{,}0005$; $^{\#\#}p \leq 0{,}00001$; $^{\#\#\#}p \leq 5 \times 10^{-6}$.

folds constant factor, thus $K_{m2} = 7^2\ K_{m1}$. Conversely, no equation to fit V_{max} with the length of the $(PO_4^-)_n^=$ was found (Fig. 2b, middle plot), while a second-order polynomial in *n* fit the slope k_{m1}/V_{max1} for the high-affinity and a linear regression for lower affinity K_{m2}/V_{max2} (Fig. 2b, right plot) was found.

The velocity of $PO_4^{\equiv}$ produced from a given $(PO_4^-)_n^=$ can be written as shown in Equation (1). We determined the kp_n from the slope of the natural logarithm of the concentration of the product ($PO_4^{\equiv}$) versus time (Fig. 2c), and it was a first-order velocity constant with regards to $(PO_4^-)_n^=$ Eq. (2).

$$v = kp_n[E(PO4_n^-)^=] \tag{2}$$

3.3. Longer polyphosphates (n) were hydrolyzed before than the shorter (n-1) length

To investigate the mechanism for of $PO_4^{\equiv}$ release from $(PO_4^-)_n^=$ we proposed that $(PO_4^-)_n^=$ were hydrolyzed in a sequence of partial reactions of the enzyme binding $(PO_4^-)_n^=$ *to* form the intermediary complex enzyme-substrate $E(PO_4^-)_n^=$, and then $PO_4^{\equiv}$ released, plus a shortened $(PO_4^-)_{n-1}^=$ Eq. (3) until $(PO_4^-)_2^=$ is released Eq. (4), (5)

$$(PO_4^-)_n^= + E + H_2O \overset{Kmn}{\leftrightarrow} [E(PO_4^-)_n^=] \overset{kpn}{\rightarrow} E + PO_4^{\equiv} + (PO_4^-)_{n-1}^= \tag{3}$$

$$(PO_4^-)_{n-1}^= + E + H_2O \overset{Km(n-1)}{\leftrightarrow} [E(PO_4^-)_{n-1}^=] \overset{kp(n-1)}{\rightarrow} E + PO_4^{\equiv} + (PO_4^-)_{n-2}^= \tag{4}$$

$$(PO_4^-)_3^= + E + H_2O \overset{Km3}{\leftrightarrow} [E(PO_4^-)_3^=] \overset{kp3}{\rightarrow} E + PO_4^{\equiv} + (PO_4^-)_2^= \tag{5}$$

$$(PO_4^-)_n^= + E + (n-2)H_2O \overset{Kmt}{\leftrightarrow} \sum_{i=0}^{n-3} [E(PO4_{n-i}^-)^=] \overset{kept}{\rightarrow} E + (n-2)\ PO_4^{\equiv} + \ldots + (PO_4^-)_2^= \tag{6}$$

$$Kmt = \frac{[E(PO4_n^-)^=]}{[E][(PO4_n^-)^=]} \tag{7}$$

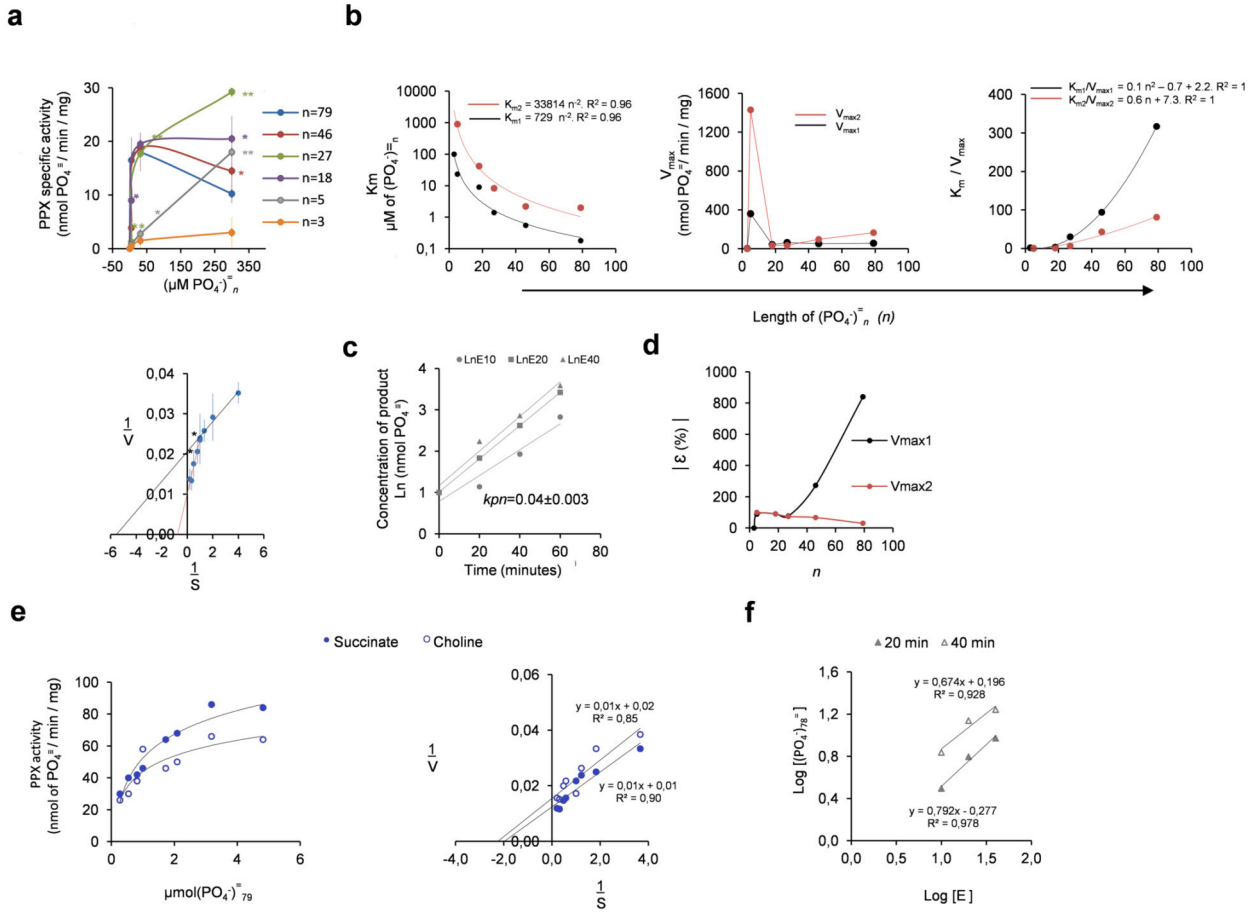

Fig. 2. Kinetic characterizations and modeling of PPX activity. **(a)** PPX activity from the periplasmic extract of *Pseudomonas aeruginosa* quantified in 100 mM acetate buffer, pH 5, 2 mM $MgCl_2$, 10 mM KCl, with polyphosphates $(PO_4^-)_n^=$ of different length as substrate, n = 6 independent experiments (Top plot). Lineweaver–Burk representative plot of $(PO_4^-)_{79}^=$ for determination of the affinity constant (Km) and maximal velocity (Vmax) of PPX for different lengths of polyphosphate (n = 3, 5, 18, 27, 45, 79). Throughout, the data are expressed as mean ± s.e.m. **(b)** Representation of K_m, V_{max}, and slope (K_m/V_{max}) obtained by linear regression from the Lineweaver–Burk plots, versus the length of the polyphosphate used as substrate. Km vs. n was fitted by potential regression of second order. The Km/Vmax vs. n plot was fitted by a second-order polynomial equation. **(c)** Quantification of the velocity constant (*kpn*) from the integrated differential rate law of first order, for 31.5 μM $(PO_4^-)_{79}^=$ and 10, 20 and 40 μl of periplasmic extract. **(d)** Representation of the error from the modeled Vmax calculated from $v = \sum_3^n \frac{0.04\ [E][(PO4_n^-)^=]}{33814n^{-2}}$ and $v = \sum_3^n \frac{0.04\ [E][(PO4_n^-)^=]}{729\ n^{-2}}$ and (b), the measured values, versus n, the polyphosphate length. **(e)** Left plot, representative PPX activity quantified in periplasmic extracts from bacteria grown in high phosphate basalt salt medium with choline or succinate. For the PPX reaction 3 μM $(PO_4^-)_{79}^=$ was used as substrate. The right plot is a Lineweaver–Burk plot of the same values. **(f)** Quantification of the flux coefficient of control for $(PO_4^-)_{79}^=$. Throughout, the data are expressed as mean ± standard error of the mean (s.e.m). Student's T-test values for one tail, unequal variances, relative to the previous data point, were: n.s, p ≥ 0,05; *p ≤ 0,05; **p ≤ 0,01.

$$\mathrm{Keq} = \frac{[PO_4^{\equiv}]^{n-2}[(PO4_2^-)^=]}{[(PO4_n^-)^=]} \tag{8}$$

Considering that the $K_{m,}$ shown in Eq. (7) measured (Fig. 2) was in the 10^{-6} digit (μM) for every substrate molecule bound as an enzyme–substrate complex, 10^6 dissociated substrates were found, Eq. (8), the concentration of $(PO_4^-)_{n-1}^=$ was in the 10^{-9} digits (nmols), and it was insignificant compared to the $(PO_4^-)_n^=$ concentration; therefore, the enzyme would have degraded the longest $(PO_4^-)_n^=$ before it degraded the $(PO_4^-)_{(n-1)}^=$. In the second example, this enzyme had lower affinity for shorter $(PO_4^-)_{n-1}^=$ (Fig. 2b). Consequently, the global velocity Eq. (9) for the complete hydrolysis Eq. (6) of the $(PO_4^-)_n^=$ is shown below Eq. (10):

$$\mathrm{v} = kp_n[\mathrm{E}(\mathrm{PO4_n}^-)^=] + kp_{(n-1)}[\mathrm{E}(\mathrm{PO4_{(n-1)}}^-)^=] + kp_{(n-2)}[\mathrm{E}(\mathrm{PO4_{(n-2)}}^-)^=] + \ldots + kp_3[\mathrm{E}(\mathrm{PO4_3}^-)^=] \tag{9}$$

$$\mathrm{v} = \sum_{i=0}^{i=n-3} kp(n-i)[\mathrm{E}(\mathrm{PO4_{n-i}}^-)^=] \tag{10}$$

Replacing the complex concentration of $[\mathrm{E}(\mathrm{PO4_n}^-)^=]$ obtained from Eq. (7) as shown in Eq. (11)–(13).

$$[\mathrm{E}(\mathrm{PO4_n}^-)^=] = \frac{[\mathrm{E}][(\mathrm{PO4_n}^-)^=]}{\mathrm{Kmn}} \tag{11}$$

$$[E(PO4_{(n-1)}{}^{-})^{=}] = \frac{[E][(PO4_{(n-1)}{}^{-})^{=}]}{Km(n-1)} \tag{12}$$

$$\vdots$$

$$[E(PO4_{3}{}^{-})^{=}] = \frac{[E][(PO4_{3}{}^{-})^{=}]}{Km3} \tag{13}$$

The rate equation Eq. (9) for hydrolysis of every length Eq. (14)–(16) can be written as function of the $(PO4_n{}^{-})^{=}$ concentration and the enzyme Eq. (11)–(13):

$$v_n = \frac{kpn\ [E][(PO4_n{}^{-})^{=}]}{Kmn} \tag{14}$$

$$v_{(n-1)=} \frac{kp(n-1)\ [E][(PO4_{(n-1)}{}^{-})^{=}]}{Km(n-1)} \tag{15}$$

$$\vdots$$

$$v_3 = \frac{kp3[E][(PO4_3{}^{-})^{=}]}{Km3} \tag{16}$$

$$v = \frac{kpn[E][(PO4_n{}^{-})^{=}]}{Kmn} + \frac{kp(n-1)[E][(PO4_{(n-1)}{}^{-})^{=}]}{Km(n-1)} + \cdots + = \frac{kp3[E][(PO4_3{}^{-})^{=}]}{Km3} \tag{17}$$

Equation (9) becomes Eq. (17) and can be written as Eq. (18).

$$v = \sum_{3}^{n} \frac{kpn\ [E][(PO4_n{}^{-})^{=}]}{Kmn} \tag{18}$$

The Lineweaber–Burk equation becomes Eq. (19).

$$\frac{1}{v} = \frac{\prod_{i=3}^{i=n} Km(n-i)}{\sum_{i=0}^{i=n-3}\{\prod_{h=o,h\neq i}^{h=n-3} Km(n-h)\} kp(n-i)[E][(PO4_{(n-i)}{}^{-})^{=}]} \frac{1}{[(PO4_{(n+1-i)}{}^{-})^{=}]} \tag{19}$$

Equation (17) indicates that the enzyme binds the longest $(PO4_n{}^{-})^{=}$ with higher affinity, and it will not bind the $(PO4_{(n-1)}{}^{-})^{=}$ until its concentration is much larger than $(PO4_n{}^{-})^{=}$. Thus, the second term in Equation (17) was negligible compared to the first term at the beginning of the reaction. As the reaction progresses the second term Eq. (17) becomes important and the third insignificant until most of the $(PO4_{(n-1)}{}^{-})^{=}$ was hydrolyzed. The sequence continues until the whole $(PO4_n{}^{-})^{=}$ of the same length was processed.

In a steady-state, every intermediate $(PO_4{}^{-})_{n\text{-}i}$ should be constant, and the velocity of degradation should be the same $v_n = v_{n-1} = v_{n-i} = v_3$. Since V_{max} had no function associated with the length (Fig. 2b) and remained fairly constant for n > 5, we replaced *kpn* for the value obtained in Fig. 2c and could predict the $K_{m(n\text{-}i)}$ by the equation that fit the K_m series in Fig. 2b. The final equation is a function of the number of units of the enzyme [E] and the polyphosphate concentration $[(PO4_n{}^{-})^{=}]$ for both series of K_m.

$$v_2 = \sum_{3}^{n} \frac{0.04[E][(PO4_n{}^{-})^{=}]}{33814n^{-2}} \tag{20}$$

$$v_1 = \sum_{3}^{n} \frac{0.04[E][(PO4_n{}^{-})^{=}]}{729n^{-2}} \tag{21}$$

The Lineweaver–Burks equation becomes as Eq. (22), (23).

$$\frac{1}{V} = \frac{\prod_{i=3}^{i=n} 729(n-i)^{-2}}{\sum_{i=0}^{i=n-3}\{\prod_{h=o,h\neq i}^{h=n-3} 729(n-i)^{-1.84}\} 0.04[E][(PO4_{(n-i)}{}^{-})^{=}]} \frac{1}{[(PO4_{(n+1-i)}{}^{-})^{=}]} \tag{22}$$

$$\frac{1}{V} = \frac{\prod_{i=3}^{i=n} 33814(n-i)^{-2}}{\sum_{i=0}^{i=n-3}\{\prod_{h=o,h\neq i}^{h=n-3} 33814(n-i)^{-2.4}\} 0.04[E][(PO4_{(n-i)}{}^{-})^{=}]} \frac{1}{[(PO4_{(n+1-i)}{}^{-})^{=}]} \tag{23}$$

To evaluate the accuracy of the equation, we represented the deviation of theoretical values Eq. (20), (21) from the quantified values, which showed that the Eq. (21) of V_{max2} was a better fit for higher concentrations of $(PO_4{}^{-})^{=}_n$, because it had a lower error (Fig. 2d); thus, it modeled the PPX activity better.

3.4. PPX from choline medium is anti-competitively inhibited

We also compared the effect of choline in the specific activity of PPX from bacteria grown with choline (Fig. 2e, left plot), which had a higher affinity ($K_m = 0.5$ μM) and half the maximal velocity ($V_{max} = 50$ nmol $PO_4{}^{\equiv}$ /min/mg of protein), relative to succinate, ($K_m = 1$ μM, $V_{max} = 100$ nmol $PO_4{}^{\equiv}$ /min/mg of protein). The parallel regression in the double reciprocate plot (Fig. 2e, right plot) indicated anticompetitive inhibition of PPX from choline medium, which shows an apparent higher affinity (lower Km), and half the maximal velocity because the inhibitor binds the enzyme-substrate complex Eq. (24), which consumes the complex but does not produce $PO_4{}^{\equiv}$. In this case, the enzyme has a lower affinity for the inhibitor than the complex, however since there are 2 reactions consuming $E(PO_4{}^{-})_n{}^{=}$ the affinity seems increased but part of the complex is ineffective, thus, the overall activity is decreased. This type of inhibition occurs when several substrates are reacting, and the inhibition cannot be reversed by a substrate addition [33].

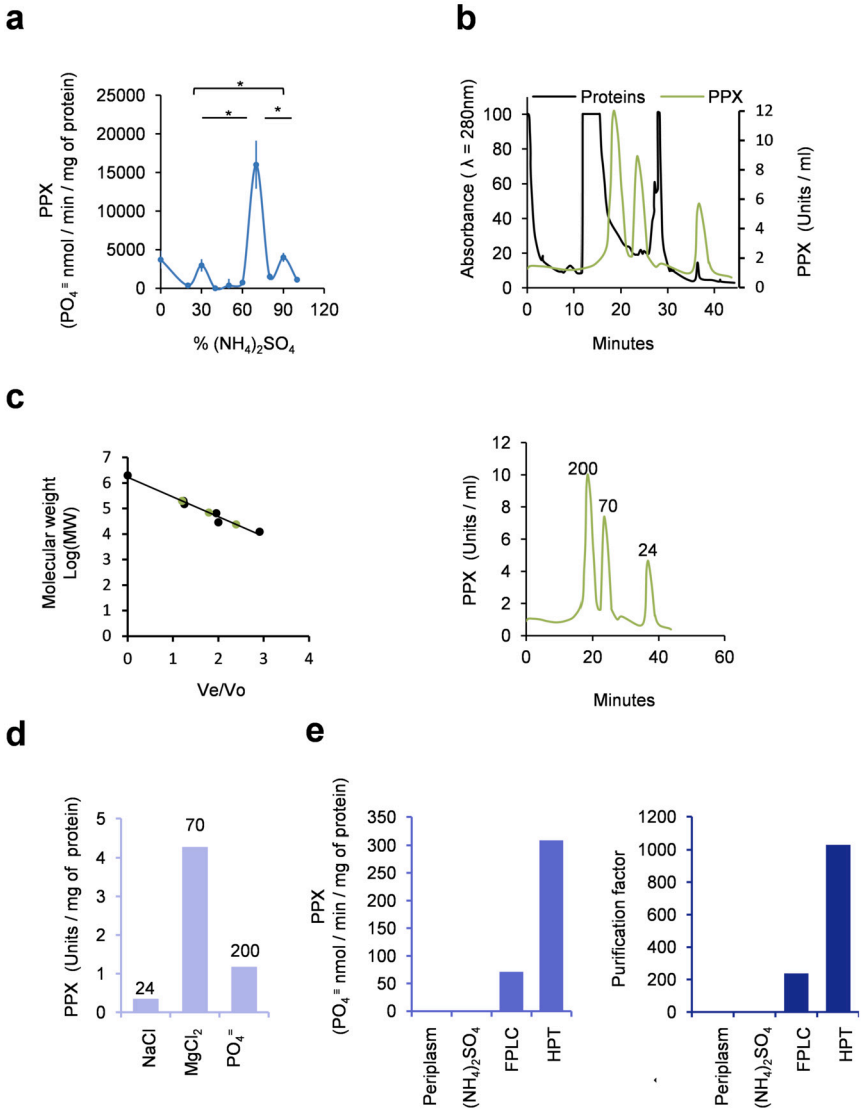

Fig. 3. Identification of PPX isoenzymes. **(a)** PPX activity was separated with $SO_4(NH_4)_2$ from 10 ml of periplasmic extract, from *Pseudomonas aeruginosa* grown with succinate. n = 3 independent experiments, data are expressed as mean ± s.e.m. **(b)** The proteins from fractions between 30-90% of $(NH_4)_2SO_4$, filtered through millipore 0.5 μm, and dissolved in 14 mM Tris-HCl were separated by molecular weight Colum Bio-sep-Sec 300 in FPLC and eluded at 1 ml/min of the same buffer, fractions of 1 ml were collected. **(c)** The FPLC column separated the proteins, by molecular weight, and was calibrated with molecular weight markers, 2000 KD, blue dextran; 200 KD, amylase; 150 KD, alcohol dehydrogenase; 66 KD, carbonic anhydrase; and 12.4 KD, cytochrome C (left plot). PPX activity, determined in 250 μl of the elution fractions, in 100 mM acetate buffer at pH 5, 2 mM $MgCl_2$, incubated at 37 °C, 40 minutes, detected by Fiske [22] (right plot). **(d)** Elution profile of the peaks resolved from (c) in hydroxyapatite (Bio-Rad, Bio-Gel HTP) in 5 mM $MgCl_2$, 150 mM NaCl or 100 mM NaH_2PO_4 solutions. **(e)** Specific activity of PPX measured in the different purification steps and their respective purification factor.

$$\begin{array}{l} E + (PO_4^-)_{79}^{=} \leftrightarrow E(PO_4^-)_{79}^{=} \rightarrow E + (PO_4^-)_{78}^{=} + PO_4^{\equiv} \\ \quad\quad + \\ \quad\quad I \\ \quad\quad \updownarrow \\ \quad\quad IE(PO_4^-)_{79}^{=} \end{array} \tag{24}$$

Considering $(PO_4^-)_{79}^{=}$ and $PO_4^{\equiv}$ both of infinite concentration, relative to the enzyme concentration, the polyphosphate metabolic pathway flux coefficient of control (Fig. 2f) were 0.79 for 20 minutes and 0.69 for 40 minutes of reaction. Indicating that 80% of the $(PO_4^-)_{79}^{=}$ degradation is controlled by PPX while 20% is by other enzymes.

3.5. Three periplasmic PPX isoenzymes

The kinetics results strongly suggest that at least two PPX enzymes in the crude periplasmic extracts exist. We then sought to separate more than one enzyme that was hydrolyzing $(PO_4^-)_n^=$ as these results also suggested two optimum pH values and a concave curve in the double reciprocal plot for PPX activity (Figs. 1b, 2a, 2b, 2d). Consistently, the protein separation from periplasmic extracts showed three peaks of enzymatic activity at 30%, 70%, and 90% of $(NH_4)_2SO_4$ (Fig. 3a). The fractions with more activity were separated by their molecular weight (MW) as shown in Fig. 3b, which also showed three peaks with PPX activity at MW 200, 70, and 24 KD (Fig. 3c). The different elution profiles from hydroxyapatite for those peaks confirmed that different proteins with PPX activity were present (Fig. 3d). The 70 KD peak eluted with $MgCl_2$, which is consistent with the fact that $(PO_4^-)_n^=$ is a highly negative polymer, such as DNA. Therefore, as with histones, it is reasonable to expect that the enzyme that binds to $(PO_4^-)_n^=$ of long chains would be a basic protein. Conversely, the protein of 200 KD elutes with a negative charge ($PO_4^{\equiv}$) indicating this could bind on $(PO_4^-)_n^=$ at basic pH 9 (Fig. 2d). The protein of 24 KD is neutral as it is eluted with NaCl and would be more active at physiologic pH 7.4 to 8 (Fig. 2d). Overall, these three purification steps achieved a purification factor of 238 and 1031 for fast protein liquid chromatography and (FPLC and HPT, respectively) as shown in Fig. 3e thus causing an increase in the specific activity from 0.3 in the periplasmic extract to 309 in HPT elutes. In this study, we identified three isoenzymes with PPX activity concurrently catalyzing the hydrolyses of $(PO_4^-)_n^=$ to produce $PO_4^{\equiv}$. These results are consistent with the low and high K_m determined, and the two optimal pH at 5.8 and 9.2 (Figs. 1b, 2a) that indicate the activity of more than one enzyme acting concurrently and under tight control as shown by the equations that fitted the K_m and V_{max}/K_m ratio with a correlation factor of $R^2 = 0.96$ (Fig. 2b).

3.6. Choline induces PPK to accumulate $(PO_4^-)_n^=$

Our previous work showed that *P. aeruginosa* changes its phosphate metabolism when this bacterium consumes choline compared to succinate, and these changes occur concurrently with changes in their glycoside and phospholipid levels [3]. When *P. aeruginosa* uses choline or its catabolites, betaine and dimethylglycine, the generation time doubles, and the $(PO_4^-)_n^=$ concentration are 5-times higher (Fig. 4a,b); these variations in $(PO_4^-)_n^=$ concentrations are dependent on the combined activity of PPX and PPK. To determine if the accumulation of $(PO_4^-)_n^=$ was due to PPX inhibition, its specific activity was quantified in bacteria grown in both media (Fig. 4c). Of note was that even though inhibited, the total PPX activity significantly increased in the periplasm of bacteria grown with choline and in membranes as compared to succinate and did not show any significant changes in the cytoplasm. Therefore, $(PO_4^-)_n^=$ accumulation may not have been due to PPX inhibition. Conversely, the PPK activity as tested in cell membranes since its location and optimal activity conditions were already known [24,25] significantly increased by 2.4-fold in choline membrane compared to succinate ($p = 0.03$) and was consistent with the 3.8-fold increase of $(PO_4^-)_n^=$ in *P. aeruginosa* grown with choline.

3.7. Relationship between the bacterial bioenergetics' and energy yield by the carbon source

The increase in PPK activity in bacteria grown with choline was consistent with the previous reports [3] of polyphosphate accumulation by choline catabolism. However, it was counterintuitive that a bacteria with 3-fold less total phosphate ($P = 0.001$) [3] and 1.3-fold less total ATP ($P = 0.32$) [3] could have 5-fold more phosphate in the form of polyphosphates ($P = 0.03$). However, the mass and energy balance indicate that the bacteria grown with choline has lower overall energy than succinate; 924 compared to 1675 μmol of ATP were consumed for the biosynthesis of macromolecules per mg of protein, respectively [3]. These results led us to hypothesize that the energy contained in the bacteria was proportional to the energy yielded by the carbon source. The theoretical values were 213 and 119 mol of ATP for succinate and choline, respectively. To further test if there were more free intracellular ATP available, in the bacteria that grew with higher energy (Fig. 4d). We measured the intracellular ATP from a calibration curve (Fig. 4e) and plotted the intracellular ATP concentration versus the energetic yield of the carbon source (Fig. 4f), which correlated with the energy yield by the carbon source ($P = 0.01$) and was significantly higher for succinate. The linear correlation as shown in Fig. 4f indicates that a higher energetic yield of the carbon source correlated with higher intracellular ATP concentration. This finding was consistent with the bacterial changes in macromolecular composition and size reduction [3] when choline is catabolized.

4. Discussion

The significant accumulation of $(PO_4^-)_n^=$ during choline catabolism [3], relative to succinate, indicated that PPX was inhibited or PPK was activated by choline. We found PPX activity was significantly higher in the periplasm (Fig. 1a) with an optimal acid pH (5.8) and a lower peak at alkaline pH (9.2) as shown in Fig. 1b. PPX was activated by Mg^{+2}, Mn^{+2}, and Zn^{+2} of 0.27 ratio of charge to radius rate (r/q), and inhibited by cations (Fig. 1c), Ce^{+3}, Fe^{+3}, Fe^{+2}, Co^{+2}, Cu^{+2} with an $r/q \leq 0.27$ and ferromagnetic properties, which further contributed to $(PO_4^-)_n^=$ accumulation and played a role in microorganism resistance to heavy metals [13]. It is known that upon infection Fe^{+2} levels are reduced in the host plasma, to levels below the optimal for bacterial growth [34]; thus, metal chelation by $(PO_4^-)_n^=$ is a bacterial survival mechanism.

Periplasmic PPX had a higher affinity for polyphosphates of the longer chain, which were hydrolyzed before the shorter ones (Fig. 2a,b). The presence of a double slope, in the double reciprocal plots (Fig. 2a,b) for every polyphosphate length tested indicates that more than one enzyme was catalyzing the polyphosphate hydrolysis. Two Km values and maximal velocity for polyphosphates of $n = 5$, 18, 27, 46, and 79 were obtained. A second-order polynomial equation was fit with the K_{m2} and provided a model for maximal velocity prediction (V_{max2}) at the highest substrate concentration with the lowest deviation from tested values (Fig. 2c,d). These

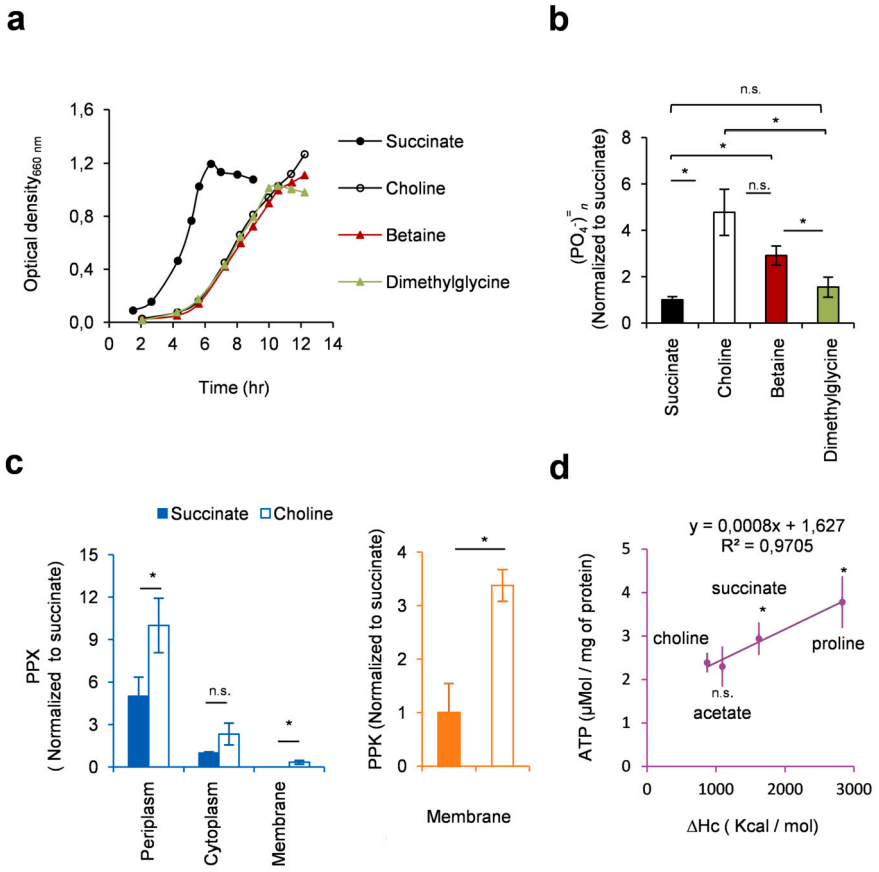

Fig. 4. (a)**R**epresentative growth curve of *Pseudomonas aeruginosa* in minimum saline medium with succinate, choline, betaine, or dimethylglycine, 20 mM as carbon plus NH_4Cl 18.7 mM. **(b)** Quantification of polyphosphates in bacteria grown with 20 mM of the intermediate metabolites of choline catabolism by *P. aeruginosa*, to an $OD_{660\ nm} = 1$; n = 3 independent experiments; values are expressed as mean ± s.e.m. **(c)** PPX activity was determined with 3 µM $(PO_4^-)_{79}^=$, 100 mM acetate buffer at pH 5, 2 mM $MgCl_2$, incubated at 37 °C, 40 minutes, detected by Fiske [22]. PPK activity from the membrane, was measured with 0.5 mg/ml $(PO_4^-)_{45}^=$ in buffer 40 mM HEPES, pH 8, 37 °C, per mg of protein. U is the amount of enzyme that catalyzes the release of 1 µmol of ADP/min. ml, per mg of protein. All values are mean ± s.e.m of three independent experiments. * $p \leq 0.05$. **(d)** Representative spectra showing luciferin–luciferase emission. Six-hundred microliters of a solution of 25 mM tricine buffer at pH 7.8, with 5 mM $MgSO_4$, 0.1 mM EDTA, 0.1 mM sodium azide, 1 mM DTT, 0.5 mM luciferin and 2.5 µL of 5 mg/ml luciferase, was added to 100 µL of ATP solution or intracellular metabolites. The emission was detected at 560 nm, without excitation, for 30 seconds after ATP addition, the emission was recorded for 300 seconds. The arrow shows the time of ATP addition. **(e)** Calibration curve for intracellular ATP quantification, obtained from the emission spectra. **(f)** Relationship between the free intracellular ATP content, from bacteria grown with different carbon sources, versus their energetic yield (ΔHc). The combustion yield was quantified by AMPAC 5.0 and compared with tabulated values to assess the error. All values are mean ± s.e.m of three independent experiments. Student's T-test values for one tail, unequal variances: n.s, $p \geq 0{,}05$; *$p \leq 0{,}05$ relative to choline.

kinetics data indicate the existence of more than one PPX enzyme in the periplasm. Consistently, the separation of the periplasmic extract by salt (Fig. 3a), molecular weight filtration (Fig. 3b), and hydroxyapatite (HTP) (Fig. 3d) produced three isoenzymes with PPX activity of molecular weights 200, 70, and 24 KD (Fig. 3c) with 238 and 1031 purification factor (Fig. 3e), relative to the periplasm, which indicates different enzymes with PPX activity are present.

Comparative studies of PPX activity from bacteria grown with choline relative to succinate (Fig. 2e) demonstrated that the bacteria had higher PPX activity, but it was inhibited in an anti-competitive manner; however, an overall higher specific activity of PPX in periplasms from choline was noted (Fig. 4c). These variations did not justify the 3.8-fold increase polyphosphate concentration in bacteria grown with choline.

In-vitro succinate is a favored carbon source (0.91 hr), but choline (1.68 hr) as shown in Fig. 4a could induce changes that render the bacteria better adapted to colonizing the lung [3–7]. This finding is consistent with a decrease in $(PO_4^-)_n^=$ when osmoprotectants, such as betaine and dimethylglycine, are catabolized (Fig. 4b). Choline has a positive charge, but when it is catabolized to betaine, a negative charge is added with the oxygen. Betaine is then transformed to neutral dimethylglycine, and both act as osmoprotectants in the hypersaline CF lung [35]. When the bacterium catabolizes choline, the positive charge from the generated by-product (NH_4^+) may be neutralized by the significant 3.8-fold increase in highly negative $(PO_4^-)_n^=$, a process that can be reduced by betaine (1.9 fold) or dimethylglycine (0.5 fold) catabolism (Fig. 4b). Thus, polyphosphates may also contribute to maintaining the electrostatic balance.

The study of the PPX and PPK activity, under nutritional conditions that replicate *in-vitro* the environment of lung infections [2], showed a significantly higher PPX activity in the periplasm, compared to the membrane, and cytoplasm (Fig. 4c, left plot).

Surprisingly, there was an overall PPX activation by choline. While the PPK activity was significantly increased 2.4-fold during choline catabolism, suggesting it is the main responsible for the significant 3.8-fold $(PO_4^-)_n^=$ accumulation (Fig. 4c, right plot). This accumulation represented 1.3% of the total phosphate and 2.9% of the total ATP [3]; thus, the energy accumulated as polyphosphate is negligible compared to that stored in the rest of the macromolecules.

These results lead us to determine the energetic yield of the catabolized carbon source and the bacterial intracellular free ATP concentration, which directly correlated (Fig. 4f) and showed a significant restriction of energy in bacteria grown with choline relative to succinate. This process was concomitant with polyphosphate accumulation and contributed to maintaining the electrostatic balance from the NH_4^+ released from choline catabolism that may facilitate bacterial migration [15]. Thus choline-induced energetic restriction may promote *P. aeruginosa* colonization by means of physiological and morphological changes that render the bacteria better fit to withstand the stress.

Author contribution statement

Sandra Grumelli: Conceived and designed the experiments; Performed the experiments; Analyzed and interpreted the data; Contributed reagents, materials, analysis tools or data; Wrote the paper.

Alejandro Rossi: Conceived and designed the experiments; Performed the experiments; Contributed reagents, materials, analysis tools or data.

Funding statement

This work was supported by CONICOR 72/95, 252/96, 417/97, 1380/97, the UNRC Res1073, Exp57803 and Rizobacter Argentina.

Data availability statement

Data included in article/supp. material/referenced in article.

Declaration of interests statement

The authors declare no conflict of interest.

Additional information

Supplementary content related to this article has been published online at https://doi.org/10.1016/j.heliyon.2022.e12601.

Acknowledgements

The authors would like to thank Dr. Carlos Domenech for permitting this research.

References

[1] V. Gupta, G.N. Kumar, A. Buch, Colonization by multi-potential *Pseudomonas aeruginosa* P4 stimulates peanut (Arachis hypogaea L.) growth, defense physiology, and root system functioning to benefit the root-rhizobacterial interface, J. Plant Physiol. 248 (2020 May) 153144, Epub 2020 Feb 26. PMID: 32172097.

[2] A. LeGouëllec, O. Moyne, E. Meynet, B. Toussaint, F. Fauvelle, High-resolution magic angle spinning NMR-based metabolomics revealing metabolic changes in lung of mice infected with *P. aeruginosa* consistent with the degree of disease severity, J. Proteome Res. 17 (10) (2018 Oct 5) 3409–3417, Epub 2018 Sep 14. PMID: 30129763.

[3] S. Grumelli, Choline triggers exacerbations of chronic obstructive pulmonary disease in patients infected with *Pseudomonas aeruginosa*, Curr. Resp. Med. Rev. 12 (2016) 167–174.

[4] S. Grumelli, Host-pathogen interaction in the lung of patients infected with pseudomonas aeruginosa, *Pseudomonas aeruginosa*, in: An Armory Within, Dinesh Sriramulu, IntechOpen, 2019.

[5] J.S. Bae, W. Lee, A.R. Rezaie, Polyphosphate elicits pro-inflammatory responses that are counteracted by activated protein C in both cellular and animal models, J. Thromb. Haemost. 10 (6) (2012 Jun) 1145–1151, PMID: 22372856, PMCID, PMC3366017.

[6] S.K. Ku, J.S. Bae, Concentration-dependent anti-inflammatory effects thrombin on polyphosphate-mediated inflammatory responses in vitro and in vivo, Inflamm. Res. 62 (6) (2013 Jun) 609–616, Epub 2013 Mar 20. PMID: 23511931.

[7] Y.A. Komarova, D. Mehta, A.B. Malik, Dual regulation of endothelial junctional permeability, Sci. STKE 2007 (412) (2007 Nov 13) re8, PMID: 18000237.

[8] A. Mitsios, A. Chrysanthopoulou, A. Arampatzioglou, I. Angelidou, V. Vidali, K. Ritis, P. Skendros, D. Stakos, Ticagrelor exerts immune-modulatory effect by attenuating neutrophil extracellular traps, Int. J. Mol. Sci. 21 (10) (2020 May 21) 3625, PMID: 32455533, PMCID: PMC7279443.

[9] L.C. Wijeyewickrema, E. Lameignere, L. Hor, R.C. Duncan, T. Shiba, R.J. Travers, et al., Polyphosphate is a novel cofactor for regulation of complement by a serpin, C1 inhibitor, Blood 128 (2016) 1766–1776.

[10] C. Puy, E.I. Tucker, Z.C. Wong, D. Gailani, S.A. Smith, S.H. Choi, J.H. Morrissey, A. Gruber, O.J. McCarty, Factor XII promotes blood coagulation independent of factor XI in the presence of long-chain polyphosphates, J. Thromb. Haemost. 11 (7) (2013 Jul) 1341–1352, PMID: 23659638, PMCID: PMC3714337.

[11] E.V. Ariskina, A.V. Vatsurina, N.E. Suzina, E.Iu. Gavrish, Kobal't- I khromsoderzhashchie vkliucheniia v kletkakh bakterii (Cobalt- and chromium-containing inclusions in bacterial cells), Mikrobiologiia 73 (2) (2004 Mar-Apr) 199–203 (in Russian), PMID: 15198031.

[12] G. Khokhlova, T. Abashina, N. Belova, V. Panchelyuga, A. Petrov, F. Abreu, M. Vainshtein, Effects of combined magnetic fields on bacteria *Rhodospirillum rubrum* VKM B-1621, Bioelectromagnetics 39 (6) (2018 Sep) 485–490, Epub 2018 May 24. PMID: 29797587.

[13] T. Kulakovskaya, Inorganic polyphosphates and heavy metal resistance in microorganisms, World J. Microbiol. Biotechnol. 34 (9) (2018 Aug 27) 139.
[14] P.I. Nikel, M. Chavarría, E. Martínez-García, A.C. Taylor, V. de Lorenzo, Accumulation of inorganic polyphosphate enables stress endurance and catalytic vigour in *Pseudomonas putida* KT2440, Microb. Cell Fact. 12 (12) (2013 May 20) 50, PMID: 23687963.
[15] M.H. Rashid, A. Kornberg, Inorganic polyphosphate is needed for swimming, swarming, and twitching motilities of *Pseudomonas aeruginosa*, Proc. Natl. Acad. Sci. USA 97 (9) (2000 Apr 25) 4885–4890, PMID: 10758151, PMCID: PMC18327.
[16] J. Ortiz-Severín, M. Varas, C. Bravo-Toncio, N. Guiliani, F.P. Chávez, Multiple antibiotic susceptibilities of polyphosphate kinase mutants (ppk1 and ppk2) from *Pseudomonas aeruginosa* PAO1 as revealed by global phenotypic analysis, Biol. Res. 48 (1) (2015 Apr 25) 22, PMID: 25907584, PMCID: PMC4424552.
[17] J.S. Bae, W. Lee, A.R. Rezaie, Polyphosphate elicits pro-inflammatory responses that are counteracted by activated protein C in both cellular and animal models, J. Thromb. Haemost. 10 (6) (2012 Jun) 1145–1151, PMID: 22372856, PMCID: PMC3366017.
[18] S.K. Ku, J.S. Bae, Concentration-dependent anti-inflammatory effects thrombin on polyphosphate-mediated inflammatory responses in vitro and in vivo, Inflamm. Res. 62 (6) (2013 Jun) 609–616, Epub 2013 Mar 20. PMID: 23511931.
[19] Y.A. Komarova, D. Mehta, A.B. Malik, Dual regulation of endothelial junctional permeability, Sci. STKE 2007 (412) (2007 Nov 13) re8, PMID: 18000237.
[20] M.M. Bradford, A rapid and sensitive method for the quantitation of microgram quantities of protein utilizing the principle of protein-dye binding, Anal. Biochem. 72 (1976 May 7) 248–254, PMID: 942051.
[21] G.F. Ames, C. Prody, S. Kustu, Simple, rapid, and quantitative release of periplasmic proteins by chloroform, J. Bacteriol. 160 (3) (1984 Dec) 1181–1183, PMID: 6501229, PMCID: PMC215841.
[22] C.H. Fiske, Y. Subbarow, The colorimetric determination of phosphorous, J. Biol. Chem. 66 (1925) 361–375.
[23] T.A. Lisa, M.N. Garrido, C.E. Domenech, *Pseudomonas aeruginosa* acid phosphatase and cholinesterase induced by choline and its metabolic derivatives may contain a similar anionic peripheral site, Mol. Cell. Biochem. 63 (2) (1984 Sep) 113–118, PMID: 6436682.
[24] M. Akiyama, E. Crooke, A. Kornberg, The polyphosphate kinase gene of Escherichia coli. Isolation and sequence of the PPK gene and membrane location of the protein, J. Biol. Chem. 267 (31) (1992 Nov 5) 22556–22561, PMID: 1331061.
[25] N.A. Robinson, H.G. Wood, Polyphosphate kinase from *Propionibacterium shermanii*. Demonstration that the synthesis and utilization of polyphosphate are by a processive mechanism, J. Biol. Chem. 261 (10) (1986 Apr 5) 4481–4485, PMID: 3007459.
[26] S. England, S. Seifter, Precipitation techniques, Methods Enzymol. 182 (1990) 285–300, PMID: 2314242.
[27] J.F. Robyt, B. White, Qualitative and quantitative methods for determining biological molecules, in: Biochemical Techniques: Theory and Practice, Monterey, California, the USA, 1987, pp. 213–251.
[28] A. Kornberg, Inorganic polyphosphate: toward making a forgotten polymer unforgettable, J. Bacteriol. 177 (3) (1995 Feb) 491–496, PMID: 7836277, PMCID: PMC176618.
[29] N.A. Robinson, H.G. Wood, Polyphosphate kinase from Propionibacterium shermanii. Demonstration that the synthesis and utilization of polyphosphate are by a processive mechanism, J. Biol. Chem. 261 (10) (1986 Apr 5) 4481–44815, PMID: 3007459.
[30] T.A. Lisa, M.N. Garrido, C.E. Domenech, *Pseudomonas aeruginosa* acid phosphatase and cholinesterase induced by choline and its metabolic derivatives may contain a similar anionic peripheral site, Mol. Cell. Biochem. 63 (2) (1984 Sep) 113–118, PMID: 6436682.
[31] I. Carter-O'Connell, M.T. Peel, D.D. Wykoff, E.K. O'Shea, Genome-wide characterization of the phosphate starvation response in *Schizosaccharomyces pombe*, BMC Genomics 13 (2012 Dec 12) 697, PMID: 23231582, PMCID: PMC3556104.
[32] K.J. Cheng, J.M. Ingram, J.W. Costerton, Interactions of alkaline phosphatase and the cell wall of *Pseudomonas aeruginosa*, J. Bacteriol. 107 (1) (1971 Jul) 325–336, PMID: 4105033, PMCID: PMC246919.
[33] A.R. Schultz, Enzymes Kinetics from Diastase to Multi-Enzyme Systems, vol. 12, 1 ed., Cambridge University Press, 1994, pp. 147–148.
[34] E.D. Weinberg, Iron and susceptibility to infectious disease, Science 184 (4140) (1974 May 31) 952–956, PMID: 4596821.
[35] M.L. Vasil, A.I. Vasil, V.D. Shortridge, Phosphate and osmoprotectants in the pathogenesis of *P. aeruginosa*, in: A.M. Torriani-Gorini, E. Yagil, S. Silver (Eds.), Phosphate in Microorganisms, American Society for Microbiology, Washington, D.C., 1994, pp. 126–132/206.